

L. E. Ramírez · C. Palacios · B. Townley ·
M. A. Parada · A. N. Sial · J. L. Fernandez-Turiel ·
D. Gimeno · M. Garcia-Valles · B. Lehmann

The Mantos Blancos copper deposit: an upper Jurassic breccia-style hydrothermal system in the Coastal Range of Northern Chile

Received: 26 April 2005 / Accepted: 6 February 2006 / Published online: 22 April 2006
© Springer-Verlag 2006

Abstract The Upper Jurassic Mantos Blancos copper deposit (500 Mt at 1.0% Cu), located in the Coastal Range of northern Chile, displays two superimposed hydrothermal events. An older phyllic alteration probably related to felsic magmatic–hydrothermal brecciation at ~155 Ma, and younger (141–142 Ma) potassic, propylitic, and sodic alterations, coeval with dioritic and granodioritic stocks and sills, and dioritic dikes. Main ore formation is genetically related to the second hydrothermal event, and consists of hydrothermal breccias, disseminations and stockwork-style mineralization, associated with sodic alteration. Hypogene sulfide assemblages show distinctive vertical and lateral zoning, centered on magmatic and hydrothermal breccia bodies, which constitute the feeders to mineralization. A barren pyrite root zone is overlain by

pyrite-chalcopyrite, and followed upwards and laterally by chalcopyrite-digenite or chalcopyrite-bornite. The assemblage digenite–supergene chalcocite characterizes the central portions of high-grade mineralization in the breccia bodies. Fluid inclusions show evidence of boiling during the potassic and sodic alteration events, which occurred at temperatures around 450–460°C and 350–410°C, and salinities between 3–53 and 13–45 wt% NaCl eq., respectively. The hydrothermal events occurred during episodic decompression due to fluid overpressuring, hydrofracturing, and sharp changes from lithostatic to hydrostatic conditions. Sulfur isotope results of hypogene sulfide minerals fall in a narrow range around 0 per mil, suggesting a dominance of magmatic sulfur. Carbon and oxygen isotopic data of calcites from propylitic alteration suggest a mantle-derived carbon and oxygen isotope fractionation due to low-temperature alteration.

Editorial handling: R. King

L. E. Ramírez (✉) · C. Palacios · B. Townley · M. A. Parada
Departamento de Geología, Universidad de Chile,
P.O. Box 13518-21, Santiago, Chile
e-mail: lramirez@cec.uchile.cl
Tel.: +56-2-9780233
Fax: +56-2-6963050

A. N. Sial
NEG LABISE Department of Geology,
Federal University of Pernambuco,
C. P. 7852,
Recife-PE, 50.732-970, Brazil

J. L. Fernandez-Turiel
Institute of Earth Sciences J. Almera, CSIC,
Sole i Sabaris,
08028, Barcelona, Spain

D. Gimeno · M. Garcia-Valles
Faculty of Geology, University of Barcelona,
Martí i Franques,
08028, Barcelona, Spain

B. Lehmann
Institut für Mineralogie und Mineralische Rohstoffe,
Technische Universität Clausthal,
Adolph Roemer Strasse 2 A,
38678 Clausthal-Zellerfeld, Germany

Keywords Cu mineralization · Upper Jurassic · Coastal range · Northern Chile

Introduction

This paper presents the results of a comprehensive and updated study of the Mantos Blancos ore deposit, in the Coastal Range of northern Chile (Fig. 1). Pre-mining resources of this deposit are estimated at 500 million metric tons with 1.0% Cu, of which 200 million tons were extracted between 1960 and 2002 (Maksaev and Zentilli 2002). The remaining ore reserves stand at 142 million tons with 0.86% Cu, and a resource of 156 million tons with 0.89% Cu (Anglo Base Metals Report, May 2003).

The Coastal Range is host to Upper Jurassic to Lower Cretaceous copper deposits of volcanic-hosted strata-bound type, and Cretaceous, generally heavily eroded porphyry-type systems, which constitute a NS-trending metallogenetic province (Camus 2003). The volcanic-hosted strata-bound ore bodies are mainly associated with hydrothermal breccia feeder structures, in which the hydrothermal breccias contain at least 50% of the economic

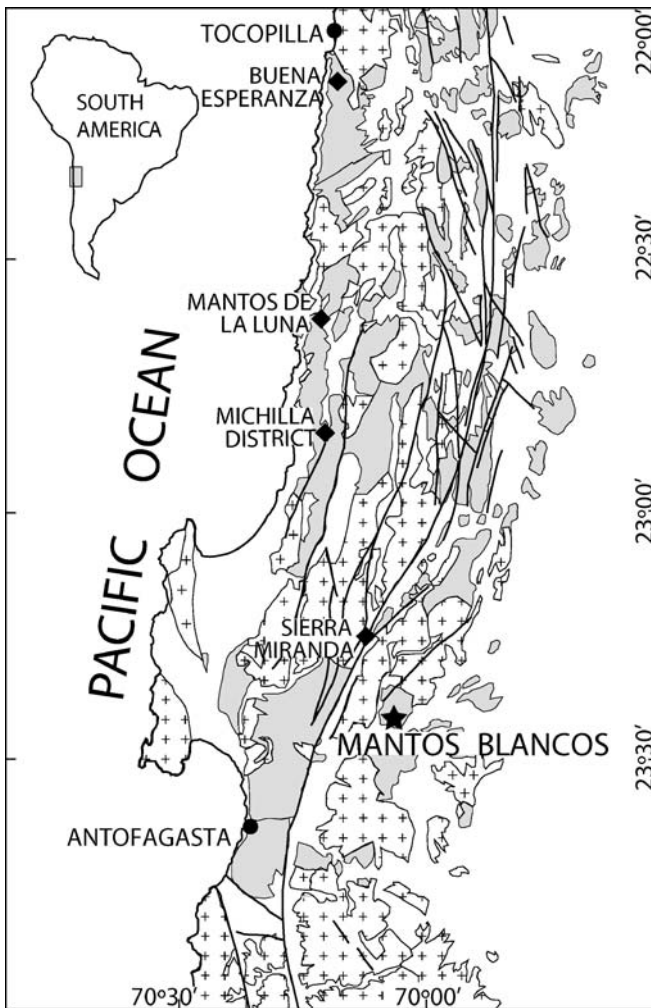


Fig. 1 Geological map of the Coastal Cordillera, Northern Chile, and location of the Mantos Blancos ore deposit (*star*) and the Upper Jurassic volcanic-hosted copper deposits (*diamonds*). In *grey* are the Middle to Upper Jurassic volcanic rocks of the La Negra Formation, crosses represent Jurassic plutonic rocks. Modified after Maksaev and Zentilli (2002)

mineralization and the highest ore grades. The hydrothermal breccias are coeval with barren and generally incipiently altered stocks and sills of mainly dioritic composition, and are intruded by late mineralization dioritic dikes.

Sulfide mineralization consists of chalcocite, digenite, bornite, chalcopyrite, and pyrite related to sodic hydrothermal alteration (Palacios 1990; Wolf et al. 1990). Most of these deposits are relatively small, with resources between 10 to 50 million tons grading 1% Cu (Espinoza et al. 1996). The porphyry-copper-type mineralization is associated with granodioritic porphyries and hydrothermal breccias, in which the hypogene mineralization consists of chalcopyrite, pyrite, and minor bornite and molybdenite, and occurs coeval with potassic and phyllic alteration (Camus 2003).

The Mantos Blancos ore body, located 30 km NE of Antofagasta, was described in the past as disseminated copper mineralization in a bimodal rhyolite-andesite

sequence by Chávez (1985), but, in general, has been considered as a strata-bound Cu deposit in recent reviews (Espinoza et al. 1996; Maksaev and Zentilli 2002). No detailed studies have been performed since 1985, when Mantos Blancos comprised a series of open pits and underground mines. During the past 20 years, the mine has been transformed into a large open-pit operation, which now provides much better geological exposures and more detailed information.

The aim of this paper is to present new data on the geology, hydrothermal alteration and mineralization, fluid inclusions, and stable isotopes, and to discuss the metallogeny and origin of the deposit.

Tectonic and geologic setting

During the Jurassic to Early Cretaceous, a subduction-related magmatic belt was established along the present Coastal Range of northern Chile. It is represented by a 7,000-m thick basaltic to andesitic volcanic pile (La Negra Formation) and granitic to dioritic plutonic rocks. The volcanic sequence evolved with time from an initial stage of tholeiitic affinity to a calc-alkaline composition (Palacios 1984; Rogers and Hawkesworth 1989; Pichowiak et al. 1990; Kramer et al. 2005). Based on radiometric age data and paleontological arguments, the extrusive event occurred between the Lower Jurassic to the Oxfordian (Rogers and Hawkesworth 1989; Gelcich et al. 2004; Kramer et al. 2005). The Jurassic volcanic pile was deposited without significant relief building, indicating considerable crustal subsidence, probably related to crustal thinning in an extensional setting (Dallmeyer et al. 1996; Maksaev and Zentilli 2002).

The intrusive rocks, also of calc-alkaline composition, include granites, tonalites, granodiorites, and diorites of Lower Jurassic to Early Cretaceous age (200–130 Ma; Scheuber and Gonzalez 1999; Oliveros 2005). Tectonic evolution of the Coastal Range during the Jurassic is interpreted in terms of coupling and decoupling between the subducting oceanic and overriding continental plates (Scheuber and Gonzalez 1999). From 195 to 155 Ma, an intra-magmatic belt was widespread, spatially related to the north–south trending, sinistral strike–slip dominant Atacama Fault Zone. However, at the end of Jurassic time, due to foundering of the subducting plate, subduction rollback, and decoupling, an east–west-trending extensional regime developed. At the end of the Jurassic to the Early Cretaceous, seismic coupling of the subducted plate is suggested by the return of the sinistral strike–slip style of deformation (Scheuber and Gonzalez 1999).

Geology of the deposit

Rock units recognized within the Mantos Blancos ore deposit consist of a rhyolitic dome and its magmatic–hydrothermal breccias, intruded by dioritic and granodioritic stocks and sills. The dioritic and granodioritic stocks

locally grade upwards into magmatic–hydrothermal breccias. These rock units are all mineralized to variable degrees. Late mafic dikes crosscut all previously mentioned rock units and are essentially barren. All the above rock units are informally grouped as the Mantos Blancos Igneous Complex (MBIC; Fig. 2). The local structural framework at deposit scale is characterized by three groups of faults: 1) NE- and NW-trending subvertical faults with evidence of sinistral and dextral movements respectively, 2) NS / 50–80° W normal faults, and 3) NS / 50–80° E normal faults.

The MBIC consists of the following major rock units:

Rhyolitic porphyry dome

The central part of the deposit consists of a rhyolitic dome (Figs. 2 and 3). The dome structure is partially preserved in the open-pit walls, but its geometry has been roughly defined from drill core logs and samples of the early stages of exploitation of the ore deposit (Chávez 1985), and later lithological modeling. Due to pervasive alteration, the contacts between different internal flows are very difficult to observe; however, near-horizontal and vertical flow

laminations are typical, varying between 1 to 4 cm in thickness. West of the pit, the felsic dome is intercalated with felsic tuffs and andesitic lava flows, and is intruded by dioritic and granodioritic sills. The rhyolitic dome consists of a rhyolite porphyry with fragments of corroded quartz and feldspar phenocrysts (1–5 mm) in an intensively altered felsic groundmass.

Rhyolitic magmatic–hydrothermal breccia system

Several sub-vertical monomictic and matrix-supported rhyolitic *magmatic* and hydrothermal breccia bodies, have been recognized within the felsic dome intrusion (Figs. 2 and 3). They consist of irregular bodies, about 100 to 250 m in vertical extent, and semi-oval to circular sections, 50 to 100 m in diameter. The matrix is composed of rhyolitic rock flour with intense alteration and disseminated sulfide minerals (Fig. 4a). The fragments are altered, irregular in shape, poorly sorted, and vary in size between 1 cm and several meters. In the centre of the ore deposit, the rhyolitic magmatic and hydrothermal breccias are intruded by late dioritic to granodioritic magmatic–hydrothermal breccias.

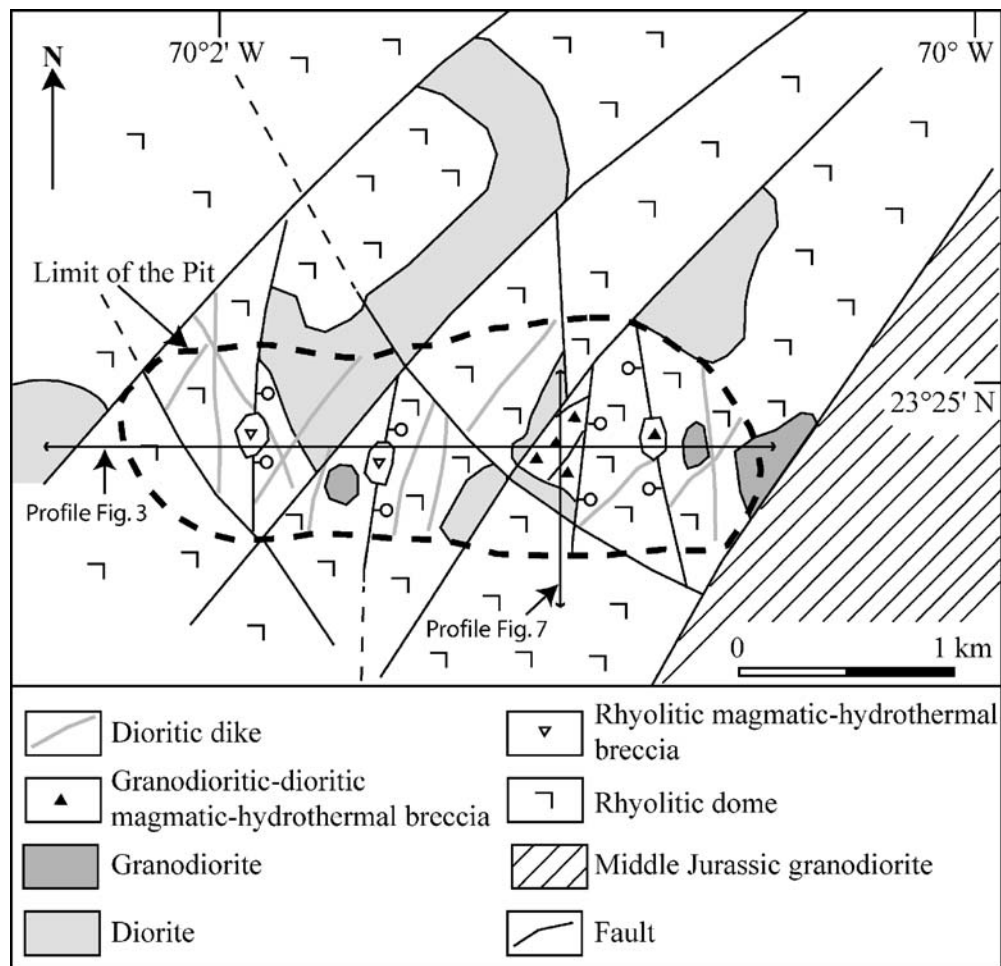


Fig. 2 Geological map of the Mantos Blancos ore deposit

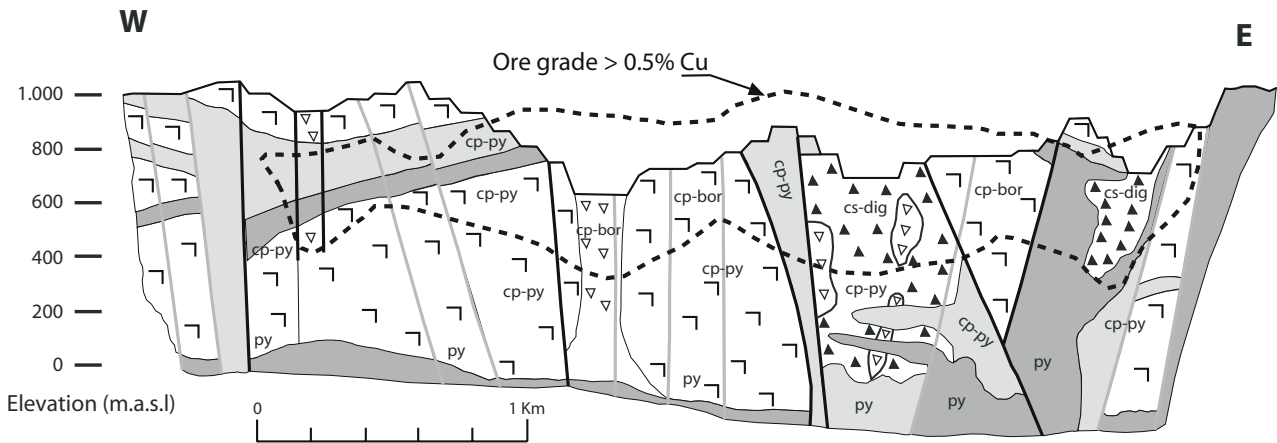


Fig. 3 E–W profile of the Mantos Blancos ore deposit. For symbols, and location of profile see Fig. 2

Bimodal stock and sill system

The rhyolite dome is intruded by a subvolcanic complex of porphyritic dioritic and granodioritic stocks and sills. At least five gently dipping sills of both rock types occur in the mine, varying in thickness between 10 and 50 m. The feeder relationship between the stocks and sills has been locally observed (Fig. 3). The granodiorite porphyry is composed of 10 to 30% phenocrysts of hornblende, plagioclase, quartz, and biotite, in a groundmass of quartz, feldspars, biotite, and hematite microlites. The diorite porphyry has 5 to 10% pyroxene and minor amphibole phenocrysts in a groundmass of fine-grained pyroxene, plagioclase, and magnetite. In both rock types, the porphyritic texture grades to aphanitic near the intrusive margins. The diorite porphyry has millimeter-size amygdules filled with quartz and quartz-sulfide. Mutual intrusive relationships between both granodioritic and dioritic rocks are common, and enclaves of one in the other have been frequently observed. The dioritic enclaves show convolute to flame-like contacts (Fig. 4b) with the host granodiorite, whereas, the granodioritic enclaves exhibit sharp or brecciated contacts with the surrounding diorite. Back-veining between the two lithological types is also observed. Recent $^{40}\text{Ar}/^{39}\text{Ar}$ data on amphibole provide ages of 142.18 ± 1.01 Ma for the granodiorite, and 141.36 ± 0.52 Ma for the diorite (Oliveros 2005).

Dioritic to granodioritic magmatic–hydrothermal breccia system

Two polymictic and matrix-supported pipe-like magmatic–hydrothermal breccias hosted within the rhyolitic dome, at the top of some dioritic and granodioritic stocks and spatially related with NS-trending faults, are recognized (Figs. 3 and 4c–e). The central and largest breccia body is crosscut by at least three metric-size sills; two dioritic and one granodioritic in composition. The breccias form near-vertical bodies, with a vertical extent of about 700 m, and diameters between 100 and 500 m. It is likely that these bodies did not reach the upper levels of the ore deposit, as

they were not observed and described in the earlier study by Chávez (1985). The upper part of the breccia pipes exhibit hydrothermal characteristics as evidenced by the presence of a matrix mainly composed of hydrothermal gangue and ore minerals. The breccia consists of altered angular and subrounded fragments of the rhyolitic dome and the granodioritic and dioritic porphyries. They are poorly sorted and range in size from 1 cm to 15 m. Downwards in the breccia bodies, magmatic features are progressively evident, with granodioritic fragments in an altered and mineralized dioritic matrix, as well as dioritic fragments in a granodioritic matrix (Fig. 4f).

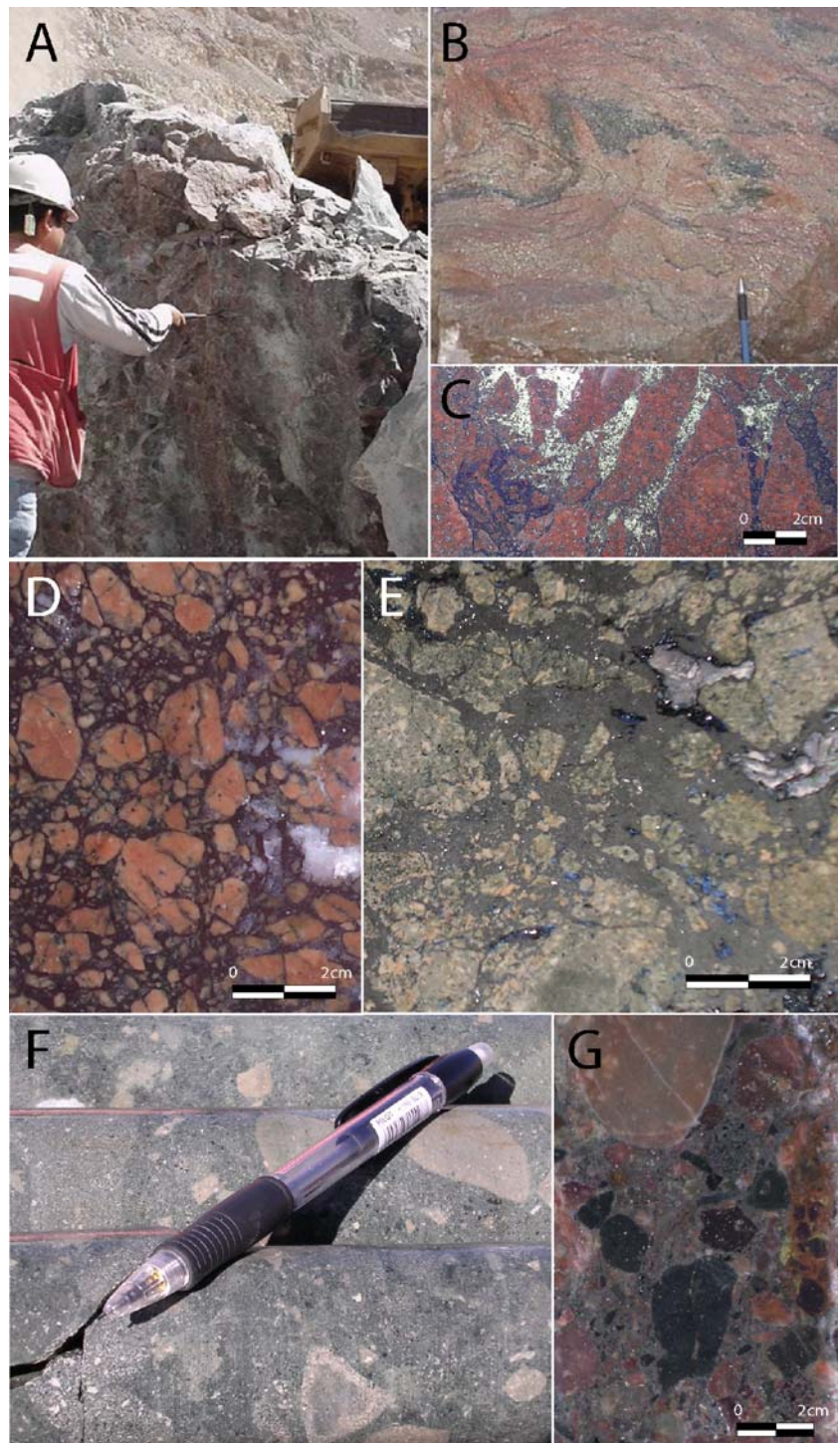
Mafic dyke swarm

Intruding all the rock units in Mantos Blancos deposit, partially altered late-ore dioritic dikes were emplaced. They are subvertical and have orientations preferentially NNE, and subordinate NS–NNW. The dikes are 1 to 12 m wide and represent about 15% of the total rock volume in the deposit. They exhibit porphyritic texture, composed of 10–25% phenocrysts of altered plagioclase, amphibole, and minor pyroxene, in a very fine-grained groundmass of feldspar, amphibole, and minor biotite and magnetite. An $^{40}\text{Ar}/^{39}\text{Ar}$ date on amphibole from a late-mineral dike in the mine is 142.69 ± 2.08 Ma of age (Oliveros 2005).

Hydrothermal alteration and mineralization

Two hydrothermal events have been recognized, based on the superimposition of alteration minerals and relationship between different stages of veinlets. The first event is represented by the rhyolitic magmatic–hydrothermal brecciation hosted by the rhyolitic dome. The second event, which represents the main stage of mineralization, is hosted mostly within the dioritic to granodioritic magmatic–hydrothermal breccias, dioritic sills, and the rhyolitic dome, and may be genetically associated with the intrusion of dioritic and granodioritic stocks.

Fig. 4 Photographs of: **a** rhyolitic magmatic-hydrothermal breccia, **b** dioritic enclave within the granodiorite showing convolute contacts, **c**, **d**, and **e** dioritic to granodioritic magmatic-hydrothermal breccias in which hydrothermal features dominate, **f** dioritic to granodioritic magmatic-hydrothermal breccia with dominating magmatic features, and **g** pebble dike



First hydrothermal event

The first hydrothermal event is characterized by the assemblage chalcopyrite, bornite, pyrite, quartz, and sericite. This assemblage occurs: 1) disseminated in the matrix of irregular and sub-vertical bodies of rhyolitic magmatic-hydrothermal breccias, 2) planar veinlets, 3) disseminated within the rhyolitic dome and in fragments of the hydrothermal breccias, and 4) as isolated crystals or as rim assemblages within and on quartz phenocrysts of the

rhyolitic dome. In the rhyolitic magmatic-hydrothermal breccias, chalcopyrite and bornite are the most abundant sulfides. Around these bodies the sulfides are chalcopyrite and pyrite. The phyllic veinlets contain the sulfide minerals as open space filling within fractures, and often display weak alteration halos of sericite and quartz. Due to the intense and widespread superimposition of the main (second) hydrothermal event, it was not possible to establish the extent and intensity of this first event. It probably extended to all rocks of the rhyolitic dome. An

$^{40}\text{Ar}/^{39}\text{Ar}$ age on sericite from this first hydrothermal event yields an age of 155.11 ± 0.786 Ma (Oliveros 2005).

Second hydrothermal event

The main hydrothermal alteration and mineralization event at Mantos Blancos is centered on the dioritic to granodioritic magmatic–hydrothermal breccias and is considered syngenetic with both breccia formation and emplacement of the granodioritic and dioritic stocks and sills. The mineralized zone extends discontinuously for 3 km in an E–W direction, has a width of up to 1 km and depth of 600 m. The hypogene mineralization occurs between the elevations of 720 and 450 m asl. (Fig. 3). Primary mineralization developed mainly within and around the magmatic–hydrothermal breccia pipes, yet the ore deposit exhibits a discontinuous lateral ore grade distribution. The highest Cu grades occur within the breccias with lateral zoning to progressively lower concentrations. This fact suggests that the magmatic–hydrothermal breccia pipes served as the feeder bodies of the main mineralization.

In the second hydrothermal event, the early alteration stage was potassic and propylitic, followed by sodic alteration. The potassic and propylitic mineral assemblages are centered on the dioritic to granodioritic magmatic–hydrothermal breccias, affecting all lithologies of the deposit. These alteration types developed pervasively, disseminated, filling amygdules within the dioritic sills, and as weak halos around flame-like veinlets that crosscut the first generation phyllic veinlets in the rhyolitic dome.

The potassic alteration is characterized by K-feldspar, quartz, tourmaline, biotite–chlorite, magnetite, chalcopyrite, digenite, and minor pyrite (Fig. 5). Relicts of K-

feldspar, tourmaline, and biotite are observed in most locations, suggesting that potassic alteration was initially widespread, but was subsequently overprinted and obliterated by later alteration stages. Dioritic and granodioritic sills, that contain amygdules filled with quartz, chlorite, digenite, chalcopyrite, and traces of K-feldspar and tourmaline, intruded the magmatic–hydrothermal breccias.

Propylitic alteration occurs extensively in the whole deposit, affecting all of the rocks (including sills and dikes), and overprinting and obliterating the potassic alteration assemblage. It occurs as disseminations and veinlets of quartz, chlorite, epidote, calcite, albite, sericite, hematite and minor chalcopyrite, galena, and pyrite. These minerals also fill amygdules within dioritic sills and dikes. Laterally, propylitic alteration consists of quartz, chlorite, epidote, and pyrite, forming a ring around the orebody at least 2 km wide. From elevations of 600 m to the upper part of the deposit, a swarm of N 25–30° E striking and sub-vertical pebble-dikes have been observed. These pebble-dikes are 10- to 20-cm thick and consist of rounded fragments of the rhyolitic dome, dioritic and granodioritic rocks, set in a matrix of quartz, epidote, calcite, galena, and pyrite (Fig. 4g).

Both potassic and propylitic alterations were followed by sodic alteration, containing albite (replacing feldspar), hematite, pyrite, chalcopyrite, and Ag-rich digenite, with minor amounts of quartz. This mineral assemblage is very extensive, centered on the magmatic and hydrothermal breccias, and occurs as disseminations, cavity fillings, and sharp veinlets. Sodic alteration and mineralization affected all lithological types between elevations of 500 m to the surface and spatially coinciding with the current commercial ore zone. Above the elevation of 500 m, the dioritic sills that intruded the magmatic–hydrothermal breccias exhibit intense stockwork with a sodic alteration mineral assemblage. As the syn-mineralization granodioritic and dioritic stocks and sills have been dated at 142.18 ± 1.01 and 141.36 ± 0.518 Ma (Oliveros 2005), respectively, and a late-ore dike yields an age of 142.69 ± 2.083 (Oliveros 2005), the age of the main hydrothermal event is constrained between 141 and 142 Ma.

Supergene oxide mineralization has been mined, with only patches of atacamite, chrysocolla, and malachite remaining. This supergene mineralization was described in detail by Chávez (1985). Although he reported primary chalcocite (late within the hypogene assemblage), our data indicate the presence of only secondary chalcocite (Fig. 6). The secondary sulfides are mainly chalcocite (forming zones of high-grade copper mineralization centered over the magmatic–hydrothermal breccia bodies, with bornite–digenite), and weak layers of covellite, together with cuprite-native copper and tenorite.

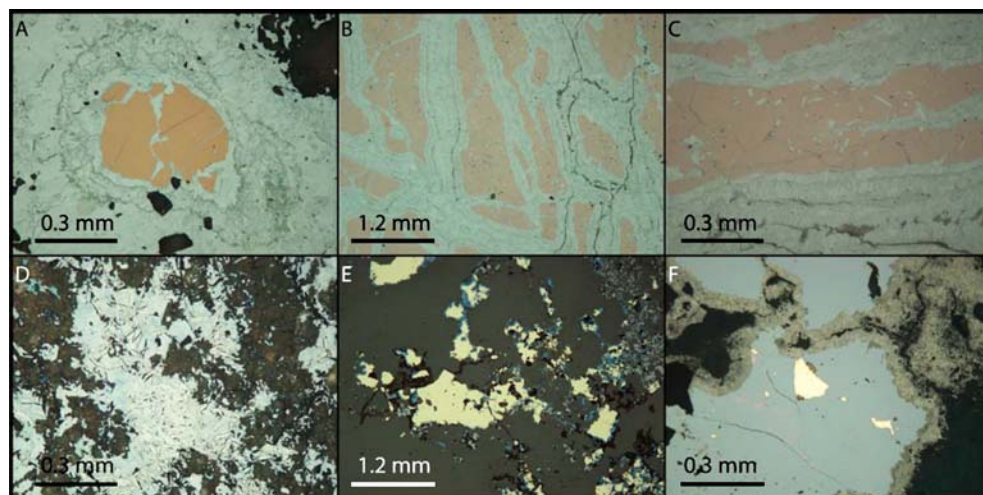
MINERALS	HYDROTHERMAL EVENTS			
	First	Second		
	Phyllic	Potassic	Sodic	Propylitic
Quartz				
Sericite				
K-feldspar				
Biotite				
Tourmaline				
Chlorite				
Albite				
Epidote				
Calcite				
Pyrite				
Magnetite				
Hematite				
Chalcopyrite				
Bornite				
Digenite				
Galena				
Magmatic and hydrothermal events	Rhyolitic dome and brecciation	Dioritic and granodioritic stocks and sills, brecciation and dike intrusion.		

Fig. 5 Hypogene mineral assemblage of the hydrothermal events at the Mantos Blancos ore deposit

Fluid inclusion studies

Fluid inclusion studies were carried out on quartz crystals of the second hydrothermal event. Samples include quartz crystals from potassic, propylitic, and sodic veinlets, and

Fig. 6 Microphotographs of **a** digenite relict in chalcocite, **b** and **c** digenite with hematite flakes replaced by chalcocite, **d** chalcocite with inclusions of hematite flakes, **e** chalcocopyrite replaced by covellite (*blue*), and **f** native copper in cuprite (*red internal reflections in grey*) with replacement rim of tenorite



from potassic and propylitic amygdules of the dioritic sills and stocks. A total of 23 samples were taken from the central part of the deposit (Fig. 7), from which 153 microthermometric measurements of primary inclusions were done. Vertical sampling extends to a depth of 850 m. Heating and freezing experiments were conducted on a Linkam THMS600 stage for homogenization temperatures (T_h) up to 450°C and on a Linkam TS1500 stage for T_h above 450°C. The uncertainty for heating runs is about $\pm 2^\circ\text{C}$ at 400°C.

Three fluid inclusion types were recognized, following the classification scheme of Nash (1976): I (liquid-dominant inclusions without halite daughters), II (vapor-dominant inclusions without halite daughters), and IIIb (vapor-dominant inclusions with halite daughters). All fluid inclusion types have mostly rounded shapes and ranged from 5 to 15 μm . No evidence was observed for

either liquid CO_2 or clathrate formation, freezing point depression measurements rule out the presence of significant CO_2 . Apparent salinities are reported in weight percent NaCl equivalent (wt% eq.), based on the halite solubility equation for halite-saturated inclusions and on the final ice-melting temperature for halite-undersaturated inclusions (Bodnar and Vityk 1994). The fluid inclusion microthermometric data are presented in Table 1 and Fig. 8. The highest temperatures were measured in types II and IIIb inclusions trapped in quartz from veinlets of the potassic alteration assemblage within the matrix of the magmatic-hydrothermal breccia at elevations between 239 and 260 m. The type-II inclusions homogenize between 550 and 608°C and have salinities of 9.9 to 10.1 wt% NaCl eq., whereas, the IIIb-type inclusions have T_h values between 530 and 590°C and salinities ranging from 52 to 74 wt% NaCl eq. The coexistence of both types of

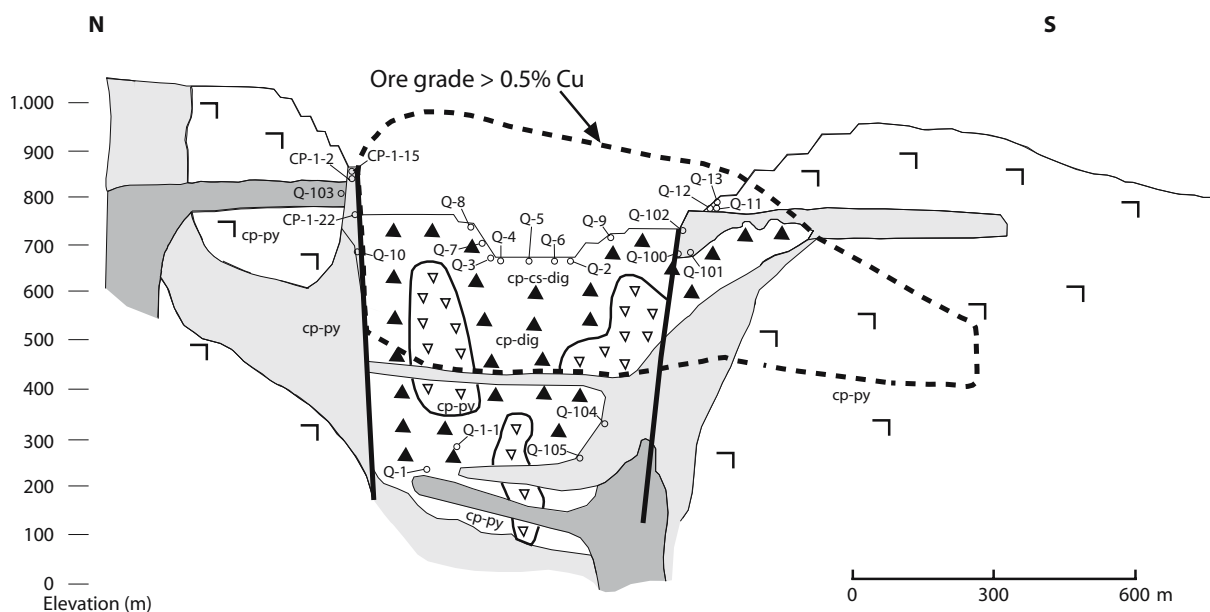


Fig. 7 N-S profile of the Mantos Blancos deposit showing the location samples used in the fluid inclusions study. For *symbols*, and location of profile, see Fig. 2

Table 1 Microthermometry data of fluid inclusions from the second hydrothermal event

Sample	Elevation (m.a.s.l.)	Size (μm)	Th (L-v) ($^{\circ}\text{C}$)	Th (Halite) ($^{\circ}\text{C}$)	%L	%V (%in)	% Halite	Tm (ice) ($^{\circ}\text{C}$)	Salinity (wt% NaCl equiv)	Remarks	N $^{\circ}$ of inclusions
Q-1	239	5–8	601 \pm 7		24 \pm 9	76 \pm 9		–6.5 \pm 0.5	9.9 \pm 0.7	Veinlets of K-assemblage in MHB	5
	239	5–9	500 \pm 20	580 \pm 10	10 \pm 5	30 \pm 4	60 \pm 5		71 \pm 3.0		5
Q-104	247	8–10	505 \pm 15		20 \pm 5	20 \pm 5		–18.0 \pm 2	19.4 \pm 3.0	Veinlets of K-assemblage in sill of dioritic porphyry	9
Q-1-1	260	5–10	564 \pm 14	550 \pm 20	23 \pm 8	77 \pm 8		–6.7 \pm 0.8	10.1 \pm 1.0	Veinlets of K-assemblage in MHB	5
	260	5–10	490 \pm 10		20 \pm 10	20 \pm 10	60 \pm 10		62 \pm 10.0		7
Q-105	260	8–10	465 \pm 12		19 \pm 6	81 \pm 5		–15.0 \pm 3.5	18.5 \pm 3.0	Veinlets of K-assemblage in sill of dioritic porphyry	5
Q-2	684	5–10	390 \pm 12	449 \pm 20	11 \pm 4	51 \pm 6	38 \pm 4		52.4 \pm 1.6	Veinlets of K-assem- blage in MHB	5
		6–10	462 \pm 8		15 \pm 10	85 \pm 10		–1.5 \pm 0.5	2.5 \pm 0.8		3
Q-3	684	5–8	404 \pm 6	464 \pm 6	10 \pm 2	50 \pm 10	40 \pm 8		53.5 \pm 0.5	Veinlets of K-assem- blage in MHB	3
		10	455 \pm 6		10 \pm 5	90 \pm 5		–2.0 \pm 1	3.3 \pm 2.5		2
Q-100	720	5–10	413 \pm 13		20 \pm 10	80 \pm 10		–19.4 \pm 1.4	22.2 \pm 10	Amygdules filled by K- assemblage in dioritic sill	5
Q-101	720	10–15	380 \pm 15		25 \pm 10	75 \pm 10		–19.4 \pm 1.4	22.1 \pm 10	Amygdules filled by K- assemblage in dioritic sill	5
Q-4	696	8–10	302 \pm 16	349 \pm 26	15 \pm 6	50 \pm 5	35 \pm 8		42.2 \pm 1.9	Veinlets of Albitic as- semblage in matrix of MHB	6
		8–10	357 \pm 23		10 \pm 6	90 \pm 6		9.9 \pm 0.9	13.9 \pm 1.1		5
Q-5	696	8	349 \pm 20	349 \pm 20	6 \pm 5	60 \pm 10	35 \pm 5		42.3 \pm 1.6	Veinlets of Albitic as- semblage in MHB	2
		8–15	346 \pm 6		9 \pm 3	90 \pm 7		–9.4 \pm 1.2	13.4 \pm 1.4		5
Q-6	696	7–10	362 \pm 8		10 \pm 5	90 \pm 5			13.2 \pm 1.8	Veinlets of Albitic assemblage in MHB	5
Q-7	708	7–10	356 \pm 11		8 \pm 2	92 \pm 2		–9.7 \pm 1.2	14.0 \pm 1.4	Veinlets of Albitic assemblage in MHB	5
Q-8	720	8–10	376 \pm 25	413 \pm 2	10 \pm 4	50 \pm 2	40 \pm 6		47.8 \pm 0.3	Veinlets of Albitic assemblage in MHB	3
		5–15	351 \pm 23		10 \pm 5	90 \pm 5		–8.8 \pm 1.8	12.6 \pm 2.2		3
Q-9	720	8	371	423	8 \pm 2	50 \pm 4	42 \pm 5		48.7	Veinlets of Albitic assemblage in MHB	1
		8–10	313 \pm 15		11 \pm 7	89 \pm 4		–8.5 \pm 1.0	12.3 \pm 1.3		5
Q-103	768	5–10	358 \pm 3		75 \pm 10	25 \pm 10		–12.5 \pm 5.0	15.3 \pm 2.5	Veinlets of K-assem- blage in sill of dacitic porphyry	6
Q-10	720	8–10	301 \pm 1		90 \pm 5	10 \pm 5		7.1 \pm 0.1	10.6 \pm 1.0	Veinlets of Propylitic assemblage in sill of dioritic porphyry	2
CP-1-22	760	8–12	218 \pm 25		65 \pm 8	35 \pm 8		–19 \pm 6.8	20 \pm 2.4	Amygdules in dioritic porphyry filled by Pro- pylitic assemblage	11
Q-11	780	8–15	269 \pm 11		70 \pm 10	30 \pm 10		–6.6 \pm 0.6	9.8 \pm 0.9	Veinlets of Propylitic assemblage in RPD	4
Q-12	780	7–12	249 \pm 5		68 \pm 12	32 \pm 12		–7.9 \pm 1.3	12.0 \pm 2.4	Veinlets of Propylitic assemblage in RPD	5
Q-102	792	8–10	335 \pm 5		90 \pm 4	10 \pm 6		–10.5 \pm 0.5	14.5 \pm 0.5	Veinlets of Propylitic assemblage in sill of dioritic porphyry	2

Table 1 (continued)

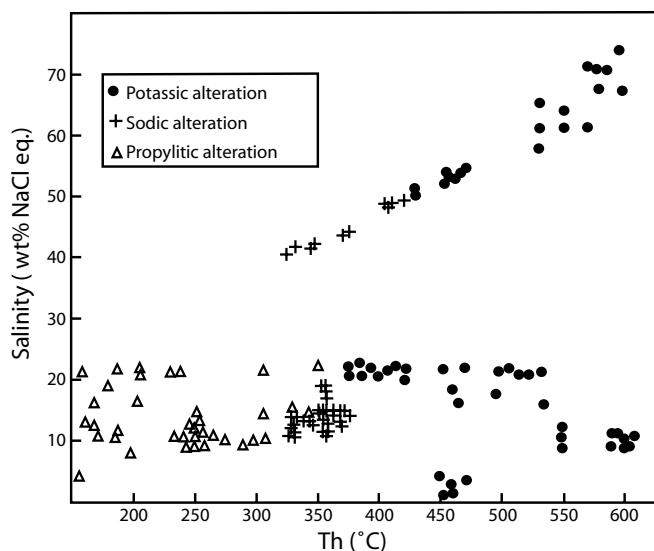
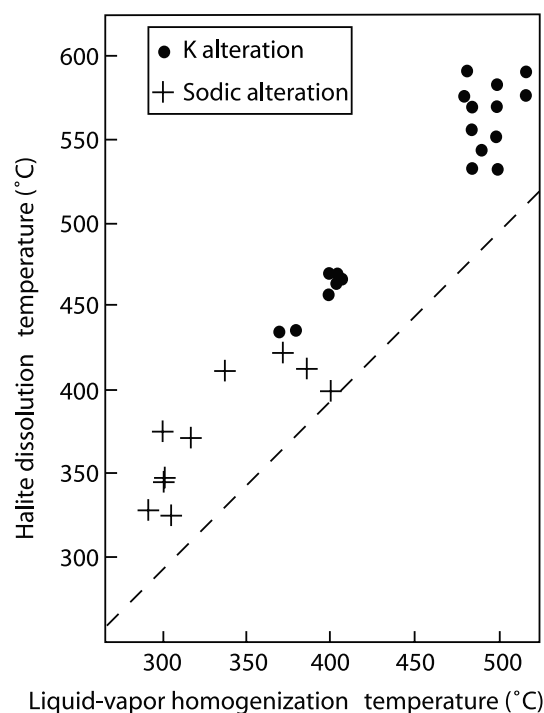
Sample	Elevation (m.a.s.l.)	Size (μm)	T_h (L-v) ($^{\circ}\text{C}$)	T_h (Halite) ($^{\circ}\text{C}$)	%L	%V (%in)	% Halite	T_m (ice) ($^{\circ}\text{C}$)	Salinity (wt% NaCl equiv)	Remarks	N $^{\circ}$ of inclusions
Q-13	792	8–10	247 \pm 3		70 \pm 5	30 \pm 5		-6.5 \pm 0.5	9.8 \pm 0.7	Veinlets of Propylitic assemblage in RPD	6
CP-1-15	816	7–11	187 \pm 35		65 \pm 10	35 \pm 10		-8.8 \pm 5.6	12 \pm 5.1	Amygdules in dioritic porphyry filled by Propylitic assemblage	6
CP-1-22	816	6–9	318 \pm 15		80 \pm 10	20 \pm 10		-10.1 \pm 1.3	14.1 \pm 1.2	Veinlets of Propylitic assemblage in dioritic porphyry	2

T_h (L-v) Liquid-Vapor homogenization temperature, T_h (Halite) halite dissolution temperature, T_m (ice) melting temperature of ice, % L, V, Halite abundance of phases at room conditions, MHB magmatic and hydrothermal breccia, RPD rhyolitic porphyry dome

inclusions within the same growth zone of a quartz crystal, is considered as indicative of deposition from boiling fluids. In these brines, T_h (halite) values are at least 60 $^{\circ}\text{C}$ greater than T_h (l-v) values in the same samples (Fig. 9). Fluid inclusion observations of samples from potassic alteration assemblages at an elevation of 684 m also display evidence of boiling: Type-IIIb inclusions have T_h values between 449 to 464 $^{\circ}\text{C}$ and salinities between 52.4 and 53.5 NaCl eq., and co-exist with vapor-rich type-II inclusions (with T_h between 462 and 415 $^{\circ}\text{C}$, and salinities between 2.5 and 3.3 wt% NaCl eq.). Also in these brines, T_h (halite) values are at least 65 $^{\circ}\text{C}$ greater than T_h (l-v) values in the same samples. Quartz crystals from potassic alteration assemblage in amygdules and veinlets from sills in the diorite contain type I and II inclusions. In these samples, T_h values decrease systematically with an increase in elevation (from an average of 515 $^{\circ}\text{C}$ at 360 m to 365 $^{\circ}\text{C}$ at 720 m). In contrast, salinities remain relatively constant (19–22 wt% NaCl eq.). Fluid inclusions associated with propylitic alteration assemblages have been measured in samples from elevations of 720 to 816 m. They correspond to type-I

inclusions, in which T_h values vary between 340 and 150 $^{\circ}\text{C}$ and salinities between 9 and 22 wt% NaCl eq.

Fluid inclusions in quartz related to the sodic assemblage were difficult to measure due to the limited amounts of albite-bearing quartz veinlets. Fluid inclusions in quartz obtained from these veinlets in the matrix of the magmatic-hydrothermal breccia at elevations between 696 and 768 m, are mainly of types II and IIIb. Evidence of boiling has been recognized at elevations of 696 to 720 m asl, in which both types of inclusions coexist in growth zones of similar hydrothermal quartz crystals. The brines have T_h values between 349 and 423 $^{\circ}\text{C}$ and salinities ranging between 42 and 48 wt% NaCl eq., whereas, the vapor-rich-two phase inclusions have T_h values between 313 and 364 $^{\circ}\text{C}$ and salinities between 13 and 14 wt% NaCl eq. Brines in the

**Fig. 8** Homogenization temperature vs salinity of fluid inclusions**Fig. 9** Halite dissolution temperature versus liquid-vapor homogenization temperature of boiled fluid inclusion samples from potassic and sodic alteration

same sample exhibit halite dissolution temperatures greater than the vapor homogenization temperatures.

Stable isotope studies

Sulfur

Seventeen sulfide samples from the second hydrothermal event were analyzed for $\delta^{34}\text{S}$ at the Scientific-Technical Services of the University of Barcelona. Sulfide samples were separated mechanically to obtain splits with 50–80 μg of sulfur. Between 100 and 300 μg of pure sulfide were mixed with V_2O_5 (1:1), homogenized and packed into high-purity tin cups. The sulfur isotopic composition was analyzed using a Continuous Flow-Isotope Ratio Mass Spectrometry (CF-EA-IRMS). Samples were combusted in an elemental analyzer (Carlo Erba EA 1108) connected to a Finnigan MAT Delta C gas mass spectrometer via a Finnigan MAT ConFlo II interface. Results are expressed in the per mil notation relative to the international Vienna-Canyon Diablo troilite (VCDT) standard. The reproducibility of measurements was $\pm 0.3\text{‰}$. The $\delta^{34}\text{S}$ values of 11 samples of pyrite, five samples of chalcopyrite, and one sample of digenite are reported in Table 2 and Fig. 10. All samples were taken in the central part of the deposit, between elevations of 450 and 780 m asl. The analyzed sulfides exhibit $\delta^{34}\text{S}$ values ranging from -5 to 1.2 per mil, with a mean value of -1.4‰ and a standard deviation of 1.8‰ . Results are similar to those previously reported by Sasaki et al. (1984) and Vivallo and Henriquez (1998). Pyrite shows the widest sulfur isotope range in comparison to the Cu-sulfides, and the variation is independent of alteration types or host rock lithology (Fig. 10).

Carbon and oxygen

Eighteen calcite samples were analyzed for $\delta^{13}\text{C}$ and $\delta^{18}\text{O}$ at the stable isotope laboratory (LABISE) of the Department of Geology, Federal University of Pernambuco, Brazil. CO_2 gas was extracted from micro-drilled powder, in a high-vacuum line after reaction with 100% orthophosphoric acid at 25°C for 1 day. CO_2 released, after cryogenic cleaning, was analyzed in a double inlet, triple collector SIRA II mass spectrometer. Results are reported relative to PDB, in per mil notation. The uncertainties of the isotope measurements were better than 0.1‰ for carbon and 0.2‰ for oxygen, based on multiple analyses of an internal laboratory standard (BSC). Values of $\delta^{13}\text{C}$ and $\delta^{18}\text{O}$ of calcite samples from propylitic alteration stage (of the second hydrothermal mineralization event) are reported in Table 3 and Fig. 11. All samples were taken in the central part of the deposit, between elevations of 172 and 900 m asl. The carbon isotope values of calcites vary between -4.37 and -6.71‰ , whereas, the $\delta^{18}\text{O}$ values fluctuate between 13.08 to 23.49‰ .

Discussion

Based on available radiometric ages and geological observations described in this study, the Mantos Blancos ore deposit was formed by two superimposed Upper Jurassic hydrothermal events. The older event occurred at ~ 155 Ma, coeval with the rhyolitic magmatic–hydrothermal brecciation and phyllic alteration. The younger event represents the main hydrothermal mineralization (~ 141 – 142 Ma) and is genetically related to dioritic and granodioritic stocks and sills and coeval magmatic–hydrothermal brecciation. Probably, both hydrothermal events contributed to extensive but irregularly distributed ore grades of hypogene mineraliza-

Table 2 Sulfur isotope of sulfides from the main hydrothermal event at the Mantos Blancos ore deposit

Sample no.	Mineral	$\delta^{34}\text{S}_{\text{CDT}}(\text{‰})$	Hydrothermal alteration ^a	Lithology ^b
M-25	Pyrite	-2.0	Propylitic	Granodiorite
CPM-54	Pyrite	-1.9	Potassic	Diorite
CP-122	Pyrite	-2.6	Sodic	Diorite
CPM-53	Pyrite	-4.0	Propylitic	Rhyolitic dome
M-3	Pyrite	1.2	Propylitic	MHB
M-4-A	Pyrite	0.7	Propylitic	MHB
BC-708	Pyrite	-0.1	Potassic	MHB
P-2-1	Pyrite	-0.3	Potassic	MHB
C-684	Pyrite	-1.1	Potassic	MHB
N-684	Pyrite	-1.2	Potassic	MHB
M-24	Pyrite	-5.0	Propylitic	MHB
M-25	Chalcopyrite	-2.1	Propylitic	Granodiorite
CPM-54	Chalcopyrite	-0.5	Potassic	Diorite
CPM-54a	Chalcopyrite	-2.0	Potassic	Diorite
CPM-53	Chalcopyrite	-4.5	Potassic	Rhyolitic dome
BC-708	Chalcopyrite	-1.3	Potassic	MHB
CPM-54a	Digenite	-3.2	Potassic	Diorite

^aHydrothermal alteration stage associated with the analyzed sulfide

^bHost rock of the sulfide
MHB Magmatic Hydrothermal Breccia

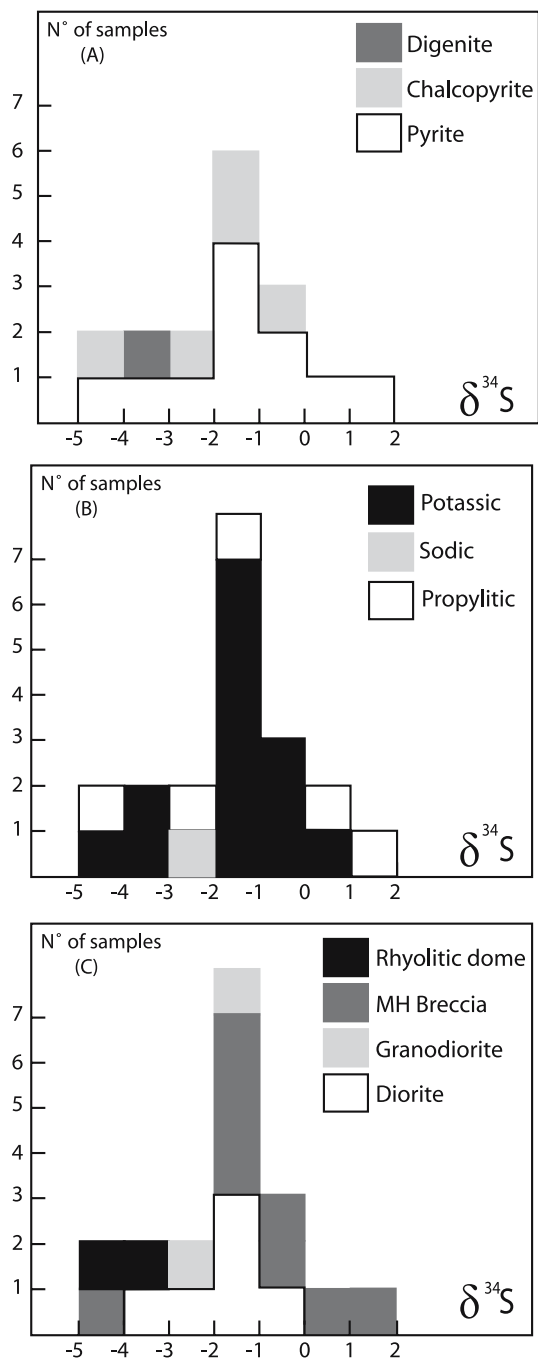


Fig. 10 $\delta^{34}\text{S}$ (‰) values of sulfides from the main hydrothermal event at the Mantos Blancos ore deposit (a). Diagrams b and c show the types of alteration and host rock, with which the sulfides are related

tion. High-ore-grade mineralization is restricted to the upper part of the magmatic–hydrothermal breccias from the second hydrothermal event. The radiometric ages for the two hydrothermal events reported by Oliveros (2005) agree with previous $^{40}\text{Ar}/^{39}\text{Ar}$ (total gas in albite) and whole rock Rb–Sr (errorchrons in strongly altered samples) radiometric ages (150–146 Ma; Munizaga et al. 1991; Tassinari et al. 1993).

The younger event is characterized by three types of alteration and mineralization: an early potassic, a propyl-

Table 3 C and O isotope analyses (‰) of calcites from the Mantos Blancos ore deposits

Sample	$^{18}\text{O}_{\text{SMOW}}(\text{‰})$	$^{18}\text{O}_{\text{PDB}}(\text{‰})$	$^{13}\text{C}_{\text{PDB}}(\text{‰})$
56-585	14.98	-15.40	-6.16
56-590	17.42	-13.04	-6.69
VB-1	18.74	-11.71	-5.50
97-230	23.49	-7.14	-6.58
VB-2	17.60	-12.86	-5.36
06-268	13.27	-16.44	-5.13
06-335	15.87	-14.54	-6.27
BC-1	13.91	-16.44	-5.13
33-200	16.72	-13.71	-6.91
33-257	20.81	-9.75	-5.72
33-288	19.87	-10.66	-4.37
33-298	13.08	-17.25	-6.02
DV-1	14.59	-15.78	-5.09
1-14B	16.51	-13.92	-6.017
696-41	13.88	-16.47	-6.17
1-14C	16.68	-13.75	-5.42
CPM1-21	16.85	-13.60	-4.75

itic, and a late sodic stage. The potassic and propylitic alteration stages coeval with dioritic and granodioritic porphyry stock intrusions, magmatic–hydrothermal breccias and late sill and dike emplacements. The late sodic alteration that developed centered around the magmatic–hydrothermal breccias, associated with intense fracturing and brecciation (including in the sills) and the main mineral deposition. The ore grade, alteration, and the copper sulfide mineral zoning indicate that the magmatic–hydrothermal breccia bodies represent the feeders to the hydrothermal system. The hydrothermal activity, was followed by the intrusion of a dioritic dike swarm. An indication of local subsidence is the common occurrence of sills intruded by vertical dikes as part of the same magmatic event. Because the magmatic pressure must exceed the least main horizontal stress and the tensile strength of the rock cover to form discordant intrusions, these intrusive

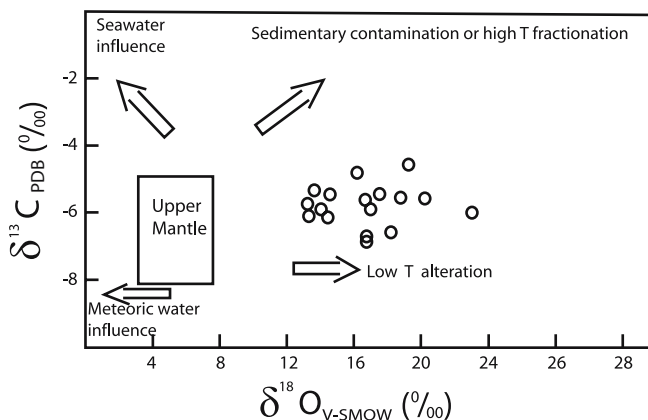


Fig. 11 $\delta^{13}\text{C}$ (‰) vs $\delta^{18}\text{O}$ (‰) diagram showing the distribution of calcites from the Mantos Blancos ore deposit. Fields and arrows after Taylor et al. (1967) and Keller and Hoefs (1995)

relationships between sills and dikes are an indication that sufficiently thick magmatic overburden was progressively formed to produce a change of the least principal stress from vertical to horizontal (Parada et al. 1997). As this sill-dike relationship has been observed at Mantos Blancos, it is suggested that the tectonic setting during mineralization corresponded to a local extensional regime, probably related to a transtensional faulting within the Atacama Fault System.

Evidence of boiling associated with potassic alteration has been found in samples up to an elevation of 684 m asl. At this elevation, fluid inclusions T_h values exceed 450°C. At such temperatures, rocks in the hydrothermal system behave in a ductile manner: with strain rates smaller than 10^{-14} /s, rocks of dioritic or granodioritic compositions behave quasi-plastically, making brittle fracturing difficult and allowing fluid pressure to approach lithostatic values (Fournier 1991, 1999). As a consequence, the magmatic-hydrothermal breccias most likely did not reach the paleosurface, and the hydrothermal system mostly formed at lithostatic pressure. The hydrothermal fluids within the magmatic-hydrothermal breccias evolved along a cooling trend, as indicated by the fluid inclusion data in quartz of the propylitic assemblage.

The emplacement of dioritic and granodioritic sills crosscutting the magmatic-hydrothermal breccias at different levels, sealed the hydrothermal system, over-pressured the fluids, hydrofractured the rocks, and produced the sodic boiling. The thermodynamic evolution of brine into the field of gas+solid salt at 350–400°C (conditions under which sodic alteration associated boiling occurred), has important implications regarding the concentration of HCl that may be transported when and if steam escapes into the overlying rocks. Fournier and Thompson (1993) noted an abrupt increase in the concentration of HCl° in steam when NaCl begins to precipitate at pressures below 300 bars. This increase occurs because hydrolysis reactions that produce HCl° and NaOH by the reaction of NaCl with H₂O become important only at pressures sufficiently low for halite (and probably also NaOH) to precipitate (Fournier and Thompson 1993). In addition, an order of magnitude higher than HCl° concentration is obtained at comparable pressures and temperatures when quartz is present. This occurs because quartz reacts with NaOH to form albite at the expense of K-feldspar or plagioclase (Fournier and Thompson 1993). The limited amounts of quartz-bearing albite veinlets in the deposit support this model.

In addition, as fluids migrated away from the early heat source (the magmatic-hydrothermal breccias) and down a thermal gradient, K-feldspar was the stable alteration mineral, as reflected by potassic alteration. The reverse reaction operated when fluids migrated away from a second heat source (intrusion of sills), conditions under which the albite stability field expanded at the expense of K-feldspar (Hezarkhani et al. 1999; Simmons and Browne 2000). Both processes probably occurred at Mantos Blancos, in which the entire evolution points to a prograde (potassic and propylitic)-retrograde (sodic) hydrothermal

sequence. These results can be interpreted as boiling events and associated decompression occurring episodically due to fluid over-pressuring, hydrofracturing, and sharp changes from lithostatic to hydrostatic conditions.

The sulfur isotopic results from hypogene sulfides suggest a largely magmatic source for sulfide sulfur and indicate a co-genetic relationship for the analyzed sulfide minerals. C–O isotopes in fresh calcite crystals reported in this paper suggest C of magmatic origin, probably of mantle provenance (Cartigny et al. 1998), and fractionation of O following the trend of low-temperature alteration caused by magmatic-hydrothermal fluids.

Acknowledgements This study was funded by a FONDEF (CONICYT, Chile), grant DOI-1012, awarded to the authors and the Mantos Blancos division of Anglo American Chile. Permission for publication was granted by the University of Chile, the Chilean Government, and Anglo American Chile. We thank the Mantos Blancos mine geology staff, especially to Jorge Pizarro, with whom we had the pleasure of working. Special acknowledgement to Jens Wittenbrink for his constructive comments to the manuscript. Finally, this paper was improved through the valuable reviews of Shoji Kojima, Robert King and Larry Meinert.

References

- Bodnar RJ, Vityk MO (1994) Interpretation of microthermometric data for H₂O–NaCl fluid inclusions. In: De Vivo B, Frezzotto ML (eds) Fluid inclusion in minerals: methods and applications. VPI, Blackburg, Virginia, pp 117–130
- Camus F (2003) Geología de los sistemas porfíricos en los Andes de Chile. SERNAGEOMIN, Chile, p 267
- Cartigny P, Harris JW, Javoy M (1998) Eclogitic diamond formation at Jwaneng: no room for a recycled component. *Science* 280:1421–1424
- Chávez W (1985) Geological setting and the nature and distribution of disseminated copper mineralization of the Mantos Blancos district, Antofagasta Province, Chile. Ph.D Thesis, University at California, Berkeley, USA, p 142
- Deines P (1989) Stable isotope variations in carbonatites. In: Bell K (ed) Carbonatites—genesis and evolution. Unwin Hyman, London, pp 301–359
- Dallmeyer RD, Brown M, Grocott J, Taylor GK, Treolar PJ (1996) Mesozoic magmatic and tectonic events within the Andean plate boundary zone, 26°–27°30' S, North Chile: Constraints from ⁴⁰Ar/³⁹Ar mineral ages. *J Geol* 104:19–40
- Espinoza S, Véliz H, Esquivel J, Arias J, Moraga A (1996) The cupriferous province of the Coastal Range, Northern Chile. In: Camus F, Sillitoe RH, Petersen R (eds) Andean copper deposits: new discoveries, mineralization, styles and metallogeny. *Econ Geol, Spec Publ* 5:19–32
- Fournier RO (1991) The transition from hydrostatic to greater than hydrostatic fluid pressure in present active continental hydrothermal systems in crystalline rock. *Geophys Res Lett* 18: 955–958
- Fournier RO (1999) Hydrothermal processes related to movement of fluid from plastic into brittle rock in the magmatic-epithermal environment. *Econ Geol* 94:1193–1212
- Fournier RO, Thompson JM (1993) Composition of steam in the system NaCl–KCl–H₂O–quartz at 600°C. *Geochim Cosmochim Acta* 57:4365–4375
- Gelcich S, Davis DW, Spooner ET (2004) Onset of Early Jurassic magmatism in northern Chile: precise U–Pb zircon ages for the La Negra Formation and the Flamenco Pluton in the Coastal Cordillera of Chañaral. Proc. IAVCEI General Assembly, Pucón, Chile (Electronic version)

- Hezarkhani A, Williams-Jones AE, Gammons CH (1999) Factors controlling copper solubility and chalcopyrite deposition in the Sungun porphyry copper deposit, Iran. *Miner Depos* 34: 770–783
- Keller J, Hoefs J (1995) Stable isotope characteristics of recent carbonatites. In: Bell K, Keller J (eds) *Carbonatite volcanism*. *Proc Volc* 4:113–123
- Kramer W, Siebel W, Romer R L, Haase G, Zimmer M, Ehrlichmann R (2005) Geochemical and isotopic characteristics and evolution of the Jurassic volcanic arc between Arica (18° 30' S) and Tocopilla (22° S), North Chilean coastal range. *Chemie der Erde. Geochemistry* 65:47–78
- Maksaev V, Zentilli M (2002) Chilean stratabound Cu–(Ag) deposits: an overview. In: Porter TM (ed) *Hydrothermal iron oxide copper–gold and related deposits: a global perspective 2*. PCG, pp 185–205
- Munizaga F, Ramírez R, Drake R, Tassinari C, Zentilli M (1991) Nuevos antecedentes geocronológicos del yacimiento Manos Blancos, Región de Antofagasta, Chile. In: *Proceedings of the 6th congress on geology, vol. 1*. Chile, pp 221–224
- Nash JT (1976) Fluid-inclusion petrology. Data from porphyry copper deposits and applications to exploration. *USGS Prof Paper* 907D, p 16
- Oliveros V (2005) Les formations magmatiques jurassiques et mineralisation du nord Chili, origine, mise en place, alteration, metamorphisme: etude geochronologique et geochemie. Ph.D Thesis. Université de Nice-Sophia Antipolis, France, p 285
- Palacios C (1984) Considerations about the plate tectonic models, volcanism, and continental crust in the southern part of the Central Andes. *Tectonophysics* 108:205–214
- Palacios C (1990) Geology of the Buena Esperanza copper–silver deposit, northern Chile. In: Fontbote L, Amstutz GC, Cardozo M, Cedillo E, Frutos J (eds) *Stratabound ore deposits in the Andes*. Springer, Berlin Heidelberg New York, pp 313–318
- Parada M, Palacios C, Lahsen A (1997) Jurassic extensional tectono-magmatism and associated mineralization of the El Faldeo polymetallic district, Chilean Patagonia: geochemical and isotopic evidence of crustal contribution. *Miner Depos* 32:547–554
- Pichowiak S, Buchelt M, Damm KW (1990) Magmatic activity and tectonic setting of early stages of Andean cycle in northern Chile. *Geol Soc Am(Specl Paper)* 241:127–144
- Rogers G, Hawkesworth CJ (1989) A geochemical traverse across the North Chilean Andes: evidence for crust generation from the mantle wedge. *Earth Planet Sci Lett* 91:271–285
- Sasaki A, Ulriksen C, Sato K, Ishihara S (1984) Sulphur isotope reconnaissance of porphyry copper and Manto type deposits in Chile and the Philippines. *Bull Geol Surv Jpn* 35:615–622
- Scheuber E, Gonzalez G (1999) Tectonics of the Jurassic–Early Cretaceous magmatic arc of the North Chilean Coastal Cordillera (22–26° S): a story of crustal deformation along a convergent plate boundary. *Tectonics* 18:895–910
- Simmons SF, Browne PR (2000) Hydrothermal minerals and precious metals in the Broadlands–Ohaaki geothermal system: implications for understanding low-sulfidation epithermal environments. *Econ Geol* 95:971–1000
- Tassinari C, Munizaga F, Ramírez R (1993) Edad y geoquímica isotópica Rb–Sr del yacimiento de cobre Mantos Blancos: relación temporal con el magmatismo jurásico. *Rev Geol Chile* 20:193–205
- Taylor HP, Frechen J, Degens ET (1967) Oxygen carbon isotope studies of carbonatites from the Laachersee district West Germany and Alno district, Sweden. *Geochim Cosmochim Acta* 31:407–430
- Vivallo W, Henriquez F (1998) Genesis común de los yacimientos estratoligados y vetiformes de cobre del Jurásico Medio a Superior en la Cordillera de la Costa, Región de Antofagasta, Chile. *Rev Geol Chile* 25:199–228
- Wolf FB, Fontboté L, Amstutz GC (1990) The Susana copper (–silver) deposit in northern Chile, hydrothermal mineralization associated with a Jurassic volcanic arc. In: Fontbote L, Amstutz GC, Cardozo M, Cedillo E, Frutos J (eds) *Stratabound ore deposits in the Andes*. Springer, Berlin Heidelberg New York, pp 319–338